Understanding soil loss in mollisol permanent gully head cuts by hydrological and hydromechanical response

Chao Ma[1], Shoupeng Wang[1], Dongshuo Zheng[1], Yan Zhang[1], Jie Tang[2], Yanru Wen[3], Jie Dong[4]

[1] School of Soil and Water Conservation, Beijing Forestry University, Beijing 100083, PR China

[2] Advanced Institute of Natural Sciences, Beijing Normal University at Zhuhai, Zhuhai 519087, China

[3] Institute of Agricultural Resources and Regional Planning, Chinese Academy of Agricultural Sciences, Beijing 100081, China

[4] Civil and Environmental Engineering Department, Clarkson University, NY, 13699, USA

Corresponding Author: Professor Chao Ma, sanguoxumei@163.com

Abstract: During permanent gully development, soil losses on steep slopes and in channel beds are typically driven by the hydromechanical response and water storage within the soil mass; however, this knowledge has been largely neglected in previous studies of gully erosion in the mollisol region of Northeast China. In this study, erosion intensities during the 111 d of the rainy season and 97 d of the snow-melting season were analyzed with respect to soil water storage, drainage capacity, and soil suction stress, supported by monitoring results of soil moisture, temperature, and precipitation, as well as experimental analysis of soil hydromechanical properties. Under the same confining stress, the mollisols in the interrupted head cut of Gully No. II increased more rapidly and dissipated pore water pressure more effectively than those at the uninterrupted head cut of Gully No. I. The combination of the soil water characteristic curve and the hydraulic conductivity function indicated that the mollisols of Gully No. II had a lower air-entry pressure and higher saturated hydraulic conductivity during the wetting and drying cycles than Gully No. I. The head cut area of Gully No. II exhibited rapid water infiltration and drainage response and high soil water storage capacity. The absolute suction stresses within the mollisols of Gully No. II was lower than that in Gully No. I, which could lead to high erosion per unit of steep slope area. Importantly, gravitational mass wasting on steep slopes was closely related to soil suction stress, and we observed a correlation between erosion per unit in the gully bed area and soil water storage. Therefore, it is more important to predict the soil loss in the permanent gully from soil water storage and the hydromechanical response of soil mass, other than sole rainfall amount. In other words, the required water storage capacity to yield runoff intensity and low suction stress would predict soil loss in the permanent gully head cut more accurately.

Keywords: Gravitational mass wasting; Soil water characteristic curve; Erosion per unit area

1 Introduction

Gravitational mass wasting refers to the downward movement of rock, regolith, and/or soil caused by gravity along the sloping top layers of the earth's surface (Evans, 2004; Allen et al., 2018). There are four types of mass wasting, based on the speed of movement of the material and the level of moisture, namely, falls and avalanches, landslides, flow, and creep (Bierman and Montgomery, 2014). They often occur in various sizes with undetermined failure planes and are affected by hydrological and hydromechanical responses (Stein and LaTray, 2002; Rengers and Tucker, 2014). On the steep slopes of permanent gullies, gravitational mass wasting involves debris-free soil falling owing to bed undercutting driven by intensive channelized flow or persistent high soil moisture (Harmon and Doe, 2001). Soil loss from gravitational mass wasting during the rainy season occurs when a steep slope loses support from debris deposits. Meanwhile, soil loss during the melting season may result from persistent low soil suction stress. In unsaturated soil mechanics, a high occurrence potential or intensive soil loss from gravitational mass wasting corresponds to low soil suction stress (Lu and Godt, 2013). It remains unclear whether soil loss from gravitational mass wasting corresponds to soil suction stress during these two stages.

Permanent gullies are initiated in locations where concentrated flows can erode and deliver bed sediments (Kirkby and Bracken, 2009; Sidle et al., 2017) and expand when gravitational mass wasting occurs following instant or constant water infiltration (Poesen et al., 2010; Tebebu et al., 2010). Permanent gully development can be determined by the topographical threshold and volumetric retreat rate of gully head cuts (Svoray et al., 2012; Guan et al., 2021; Zare et al., 2022), the gully length–area–volume relationship (Li et al., 2015 and 2017), and their function in the upstream drainage area and rainy days in different environments (Hayas et al., 2019). Soil loss from permanent gullies is largely influenced by hydrological factors (Gómez-Gutiérrez et al., 2012), such as the flow rate, total water volume, rainfall intensity and amount, and hydromechanical properties of the soil mass. Soil properties are affected by land use, plant roots, texture, and structure. The hydrological process near the head cut, the hydromechanical response of soil mass in reaction to water infiltration, and their relationship with soil loss from gravitational mass wasting remain unknown. Under natural conditions, water infiltrates either following rain events or snow/ice-melting events. The infiltration rate strongly depends on the amount and intensity of precipitation, leading to soil water storage. However, the amount of stored water varies due to the amount of rainfall and melting rate or temperature. During the snow/ice-melting season, the water infiltration duration persists longer than rain events because of prolonged soil saturation and an extended period of low soil suction stress. This may generate more soil loss owing to gravitational mass wasting. However, rain events typically generate intensive channelized flows, which erode steep slopes and trigger gravitational mass wasting. Therefore, it is challenging to compare soil loss in the two seasons. However, this issue could be addressed by considering the associated hydrological processes of head cuts and hydromechanical responses within the soil mass.

In the mollisol region of Northeast China (MEC), over 296,000 permanent gullies have developed since 1960 (Yang et al., 2017; Dong et al., 2019). Gravitational mass-wasting processes have caused rapid gully widening due to overfarming and a lack of maintenance (Wang et al., 2009). Various studies have focused on the hydrological processes affecting ephemeral gully development and volume disparities caused by rain/snow melting (Tang et al., 2022; Jiao et al., 2023), tillage practices (Xu et al., 2018; Li et al., 2021), and morphology (Zhang et al., 2016). Permanent gullies pose a greater threat to croplands than ephemeral gullies because the soil loss from permanent gully erosion can be as high as 50–65% of the total loss (Zhang et al., 2022). The relatively high area-increasing ratio is affected by the combination of permanent gullies with cropland use, a large ridge orientation angle, and a sunny orientation (Li et al., 2016; Liu et al., 2023). Tang et al. (2023) provided evidence of the rainfall threshold for permanent gully development. They found that the maximum value of 3-d accumulative rainfall best explained permanent gully bed erosion, and the cumulative value of erosive rainfall best accounted for gravitational mass wasting. However, gravitational mass wasting on the steep slope of a permanent gully can occur either during the rainy season or snow-melting season (Zhang et al., 2020; Zhou et al., 2023). Note that some studies proved that the soil loss during snow-melting season remarkably accounts for a large percentage (Hu et al., 2007 and 2009), and gully heads retreated faster than in the summer (Wu et al., 2008). Currently, the hydrological processes near the head cut and the hydromechanical response of mollisols to water infiltration in the two seasons have never been documented, and the associated soil loss from gravitational mass wasting is poorly understood. In the MEC, although the duration of the snow/ice-melting season is shorter than that of the accumulated rainy days (Wang et al., 2021; Fan et al., 2023; Went et al., 2024), the time for snow-melting water significantly exceeds that of rainy water infiltration. Therefore, soil water storage may surpass drainage owing to continuous meltwater infiltration and limited water drainage paths. Rain infiltration during the summer season temporarily increases and then decreases once the rain event ceases and the water drains. Stored water significantly depends on rainfall events and the initial soil water storage (Farkas et al., 2005; Xu et al., 2018). Therefore, the duration of low soil suction stress, such as high soil moisture, differed substantially between the two seasons. Another effect is channelized water during intensive rainstorms (Wen et al., 2021), which may erode the bed and result in gravitational mass wasting. Therefore,

the soil loss from gravitational mass wasting may coincide with the soil suction stress in the snow/ice-melting season. Meanwhile, this coincidence may not exist in the rainy season.

Soil loss from gravitational mass wasting on the steep slope of a permanent gully is poorly understood in the MEC. To date, relatively few studies have addressed its relationship with the hydrological and hydromechanical response of the soil mass. This work focused on how the monitored soil water change and the suction stress affect soil loss during the rainy and melting seasons in the head cuts of two permanent gullies, where one head cut experiences no human activity, whereas the other does. Soil loss in the head cut area during the rainy and melting seasons was observed. The differences in the physical properties of the mollisols, such as pore water pressure dissipation at a given confining stress, the soil water characteristic curve (SWCC), and the hydraulic conductivity function (HCF), were compared. The soil loss per unit area on the steep slope and gully bed was analyzed for the soil water storage, drainage, and soil suction stress, respectively. The objective of this study was to characterize the relationship between soil loss intensity on steep slopes and the hydromechanical response of the soil mass, as well as the intensity in channel beds with water storage.

2 Study area

Northeast China is one of the three main mollisol regions worldwide, with a total area of 1,030,000 km^2. It contributes 20% of the grain and more than 40% of the corn in China. Most of the mollisol region was gradually converted from native vegetation to cropland beginning in the late 19th Century. Croplands constitute 80% of the total land area, and the main crop types are soybean and corn. The study area is located in the typical heavy gully erosion area of the mollisol region of Northeast China, where native grasslands and forests have been fully converted into croplands since 1968. It is situated in a transitional rolling hilly area extending from the Songnen Plain to the Greater Khingan Mountains in the west, the Lesser Khingan Mountains in the north, and near the Nen River (Fig. 1a). Owing to the gentle landscape, the farmland in the study area is covered by a thick black organic soil layer, with sandstone, mudstone, and sandy conglomerate underneath.

The two permanent gullies examined in this work are 1.4 km apart and are located on the south-facing and north-facing rolling slopes, respectively (Figs. 1b and 1c). The catchment area above Gully No. I is 0.22 km^2. The relative relief and channel gradient are 25.85 m and 3.3%, respectively. The catchment above the head cut of Gully No. II is 0.35 km^2, and the relative relief and channel gradient are 26.1 m and 3.2%, respectively. The width of Gully No. I gradually broadened, whereas Gully No. II narrowed and Gully No. I was deeper (Figs. 2a and 2b). The mean depth of the Gully No. I was 3.5 m while that of Gully No. II was 1.23 m. The mean length and width of No. I gully were 25.3 m and 8.72 m, whereas those of Gully No. II were 28.2 and 5.61 m. The gully area for No. I was 199.3 m^2, and the volume was 863.6 m^3. For Gully No. I, the area and volume of the gully were 143.3 m^2 and 123.6 m^3.

The two gullies are still expanding because they are connected to the river network, which drains water into the Nen River. Although grass covers the area near the sidewall and ridge along the gully, mass-wasting movement frequently occurs during the melting and rainy seasons. The differences in the gully planform and depth indicate that the mass movement at the sidewall or head cut has distinctive rates and scales. The mass movement at the sidewalls of the two gullies differed in scale, as shown in Figs. 2c and 2d. The height and width of the Gully No. II were lower than those of the Gully No. I (Fig. 3). The head cut area of Gully No. II underwent tillage activities, whereas the head cut area of Gully No. I did not. Therefore, Gully No. II is representative of the initial development stage for a large permanent gully.

The study area has a continental monsoon climate with variable annual precipitation ranging from 347 to 775 mm, averaging 546 mm between 1971 and 2018 (Tang et al., 2023). Rainfall mainly occurs between June and August, accounting for 70–90% of the annual precipitation, with an average of 461 mm. Snowfall occurs mainly from

November to April, accounting for 10–30% of the annual precipitation. The average temperature in the coldest and warmest months are –22.5 °C and 20.8 °C, respectively, with an annual average temperature of 0 °C.

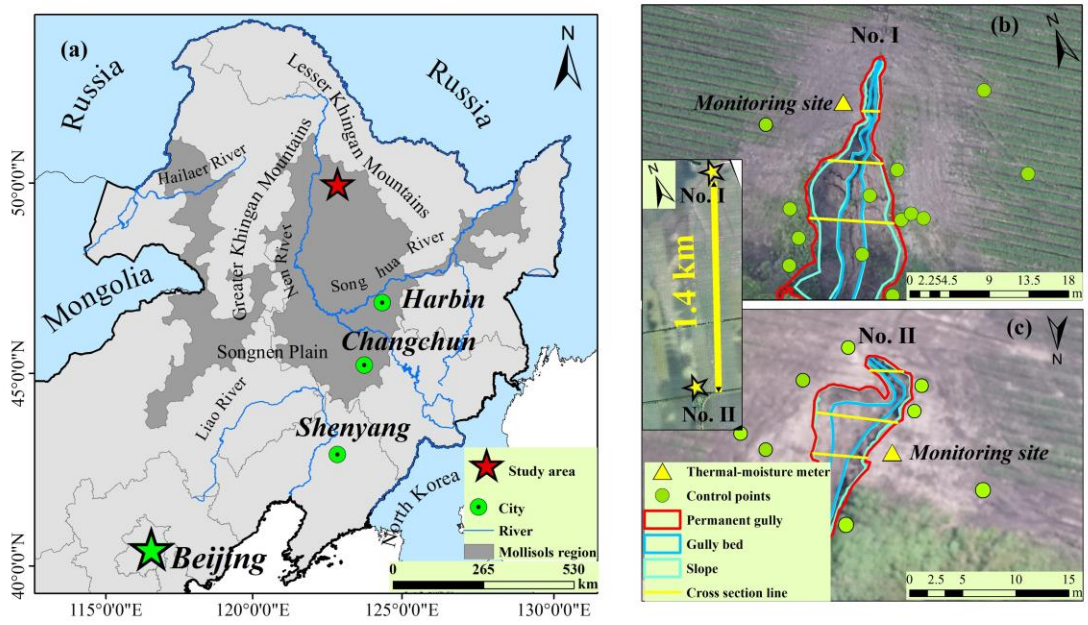

Fig. 1. Location of the two permanent gullies in the mollisol region of Northeast China. **(a)** The red star marks the observation site in the study area (from ESRI). **(b)** Monitoring sites and ground controlling points at permanent Gully No. I. **(c)** Monitoring sites and ground controlling points at permanent Gully No. II. (background of **a** is from ESRI. The area between the blue lines marks the gully bed, and that between the pink and blue lines marks the steep slope.

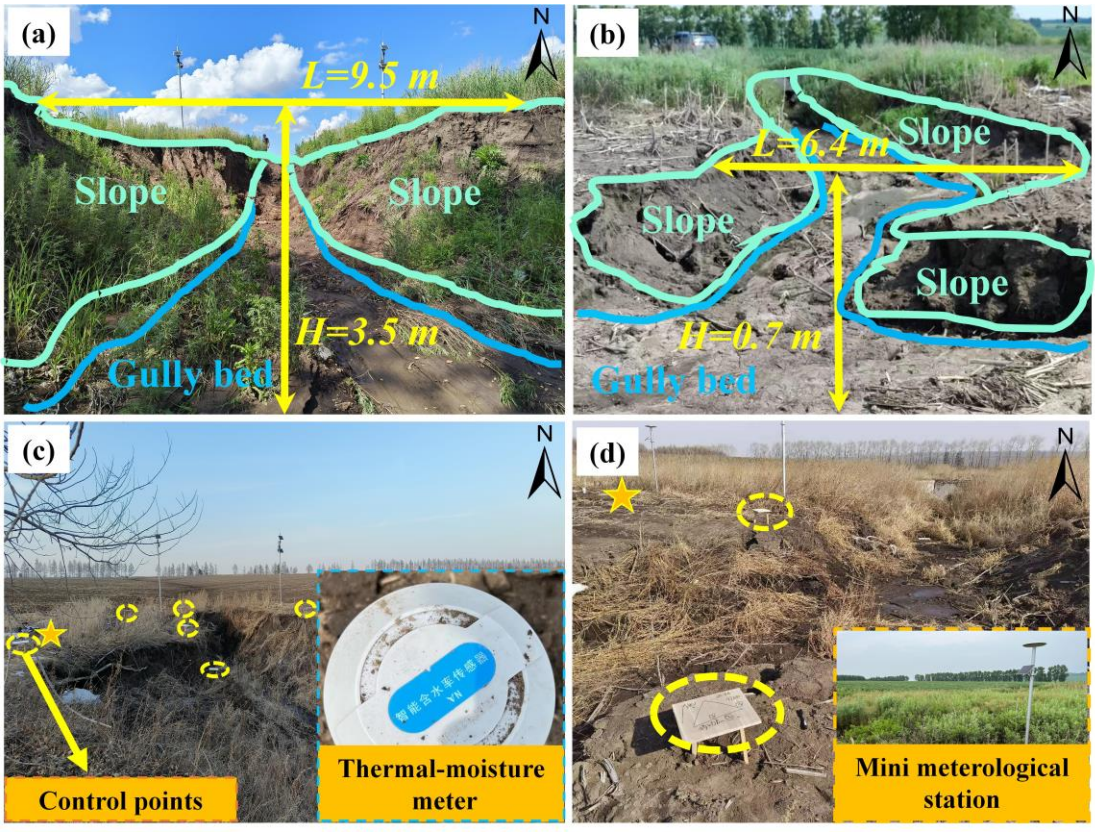

Fig. 2. A close view of the steep slope and head cut of the two permanent gullies, with **(a)** cross-section and upstream view of the permanent Gully No. I, **(b)** cross-section and downstream view of the permanent Gully No. II, (**c**) ground control points (blue dot circles) and the soil moisture–temperature monitoring site (yellow star) at permanent Gully No. I, and **(d)** ground controlling points and the soil moisture–temperature monitoring sites at permanent Gully No. II. The location of the head cut of the two gullies is shown in Fig. 1. The area between the blue lines marks the gully bed. The area between the pink and blue lines marks the slope.

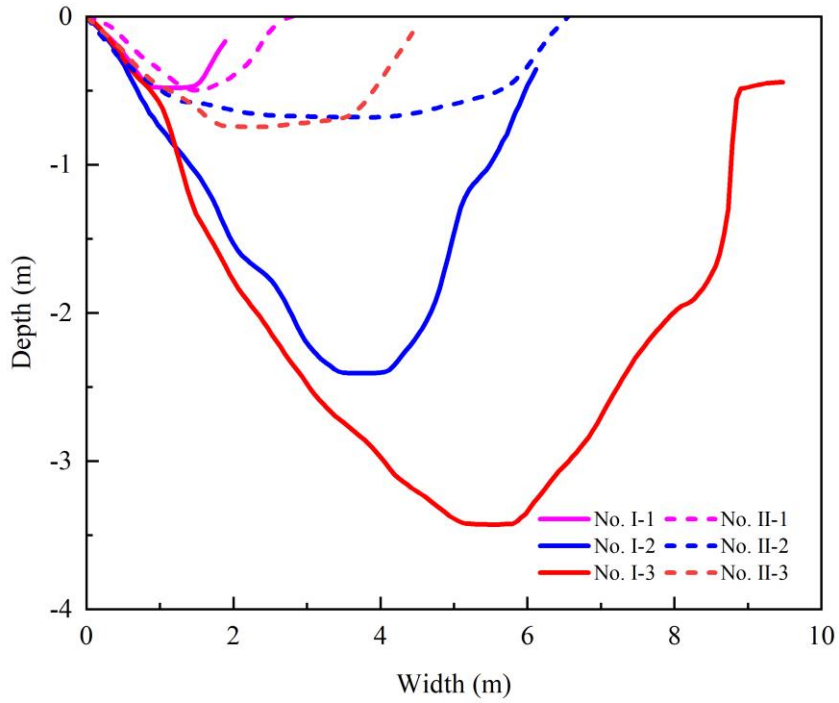

Fig. 3. Difference of the two permanent gullies' cross-section. The location of the cross-section lines is shown in Figs. 1b and 1c.

3 Material and methods

3.1 Monitoring work

Near the gully head cut, frequency–domain reflectometry sensors were installed to monitor the soil moisture and air temperature at depths of 20, 40, 60, and 80 cm (Fig. 2c). These two monitoring sites share the same rainfall records as Gully No. II (Fig. 2d). A trench was dug to obtain soil samples from the two monitoring sites. The soil samples were used for pore water pressure dissipation tests via consolidated undrained triaxial compression tests (CU) using a GDS triaxial apparatus (GDS, UK), and the unsaturated permeability was measured using the transient release and imbibition method (TRIM; Lu and Godt, 2013).

To observe the gravitational mass-wasting process during the rainy and melting seasons, the study area was scanned using numerous control points (the dots in Figs. 1a and 1b and dashed circles in Figs. 2c and 2d) installed in and around the gully area, and an unmanned aerial vehicle (UAV) was used. These control points were used to improve the accuracy of the UAV-derived map and digital elevation model to obtain highly accurate topography data. Three flights on June 28, 2022, October 17, 2022, and June 20, 2023, were performed with the same flight routine and image overlap. The two frontier flights in 2022 spanned 111 d during the rainy season. The latter two covered the winter of 2022 and the spring of 2023. As low soil moisture persists from October each year and snow cover in the winter does not result in gravitational mass movement, the effective duration of the melting season starts on March 15, 2023. Therefore, the melting season in this study lasted 97 d. We used Pix4D software to process the

image synthesis and gully topography production, which can reallocate the point cloud and filter the points of the vegetation layer. As the points of the vegetation layer, mainly the grass blades, are changeable in plant height, whereas the ground point is fixable, the vegetation layer can be filtered out and removed using the filtering tool. The DEM products were spatially registered in ArcGIS 10.2 using a standard layer of orthoimages, ground control points, and spline functions (Table 1). The erosion depth of the head cut was then obtained from the difference between the two DEMs. Therefore, the linearity and erosion per unit area could be calculated using the erosion depth and grid size. The differences between the two digital elevation models generated positive and negative terrain, which showed soil loss from gravitational mass wasting. The eroded soil volume in a unit of steep slope surface area, termed erosion per unit area, was applied to address the erosion caused by gravitational mass wasting.

Table 1. Detailed information on three UAV flights and the digital elevation models

UAV model	**F**light date	**Season/ duration**	**F**light height (m)	**DEM** accuracy **(**m)	**Image o**verlap **(**%)
DJI Inspire 2 RTK	2022.06.28	/	200	0.058	80
DJI Phantom 4 RTK	2022.10.17	Rainy/111 d	500	0.108	80
DJI Phantom 4 RTK	2023.06.21	Melting/97 d	150	0.042	80

3.2 Tests of pore water pressure rising and dissipation

The consolidation module of the GDS triaxial apparatus was used to record the pore water pressure within the soil mass under a given confining stress. The soil samples were initially saturated in a vacuum pump and then consolidated in the chamber of the GDS apparatus at effective confining pressures of 100, 200, and 300 kPa with a 10-kPa backpressure. The consolidation process was completed when the pore water pressure decreased to the backpressure values.

For the pore water increasing stage:

$$P_{\uparrow} = P_0 \times t^{b_{\uparrow}} \quad (1)$$

where $P_{\uparrow}$ is the recorded pore water pressure during the increasing stage (kPa), P_0 is the initial pore water pressure since loading (kPa), t is the time (s), $b_{\uparrow}$ is the rising proxy reflecting the steepness of the power-law curves of pore water pressure increase.

For the pore water dissipation stage:

$$P_{\downarrow} = \frac{P_{max}}{1+b_{\downarrow} \times t} \quad (2)$$

where $P_{\downarrow}$ is the recorded pore water pressure during the dissipation stage (kPa), $P_{\max}$ is the maximal pore water pressure since loading (kPa) and is the rollover point in the pore water pressure curve, t is the time (s), $b_{\downarrow}$ is the dissipation proxy reflecting the water drainage ability of soil mass at given confining pressure. It reflects the concavity of the pore water pressure dissipation curve.

3.3 Hydromechanical properties

TRIM was used to test the unsaturated permeability of the soil mass (Lu and Godt, 2013). The SWCC and HCF were obtained using Hydrus 1-D (Wayllace and Lu, 2012). Using the models proposed by Mualem (1976) and van Genuchten (1980), the constitutive relations between the suction head (h), water content (θ), and hydraulic conductivity (K) under drying and wetting states can be represented by the following equation:

$$\frac{\theta-\theta_r}{\theta_s-\theta_r}=\left[\frac{1}{1+(\alpha|h|)^n}\right]^{1-\frac{1}{n}} \quad (3)$$

and

$$K=K_s\frac{\left\{1-(\alpha|h|)^{n-1}[1+(\alpha|h|)^n]^{\frac{1}{n}-1}\right\}^2}{[1+(\alpha|h|)^n]^{\frac{1}{2}-\frac{1}{2n}}} \quad (4)$$

where θ_r is the residual moisture content (%), θ_s is the saturated moisture content (%), α and n are empirical fitting parameters, α is the inverse of the air-entry pressure head, n is the pore size distribution parameter, and K_s is the saturated hydraulic conductivity (cm/s).

Based on the observed volumetric water content and the SWCC, the suction stress (σ^s, kPa) throughout the observation stage can be expressed as:

$$\sigma^s=-\frac{S_e}{\alpha}\left(S_e^{n/(1-n)}-1\right)^{1/n} \quad (5)$$

3.4 Soil water storage and drainage

In this study, the hydrological process of the steep slope is of utmost importance for analyzing gravitational mass wasting because of the varied soil water storage and drainage in the rainy and snow-melting seasons. Soil water is temporally stored during rainstorms but drains after the rainstorms cease. The drainage process during melting is not addressed herein because melting water constantly contributes to high soil moisture. Therefore, soil water storage (S_s) during rainstorms and the snow-melting season and drainage (S_d) after a rainstorm can be evaluated using the soil depth and the difference between the maximum soil moisture and antecedent soil moisture:

$$S_e=\frac{\theta-\theta_r}{\theta_s-\theta_r} \quad (6)$$

$$S_s=S_e^w\Delta h_i \quad (7)$$

$$S_d=P-S_e^d\Delta h \quad (8)$$

where S_e is the degree of saturation, θ is the in-situ observed volumetric moisture content measured (%), Δh_i is the soil layer *i* (200 mm in this work, *i* = 1, 2, 3, 4), S_e^w and S_e^d are the residual soil moisture in the wetting and drying processes (%), and P is the accumulated rainfall (mm) and equals 0 mm in the snow-melting season. To show the soil water storage during the rainy and snowmelt seasons and the water drainage after rainfall, all the information was considered, including rainfall amount, air temperature, soil moisture, and temperature in various soil layers. The recorded rain events were categorized into four groups: light rain, moderate rain, torrential rain, and rainstorms, with rain amounts of < 10, 10–25, 25–25, and 50–100 mm, respectively.

4. Results

4.1 Erosion per unit area of gully bed and slope

The erosion per unit area in both bed and slope areas during the snowmelt season for Gully No. I was greater than that in Gully No. II (Fig. 4). This could have been driven by the low meltwater storage and high meltwater runoff at the head cut of Gully No. I. During the rainy season, the erosion per unit area for the bed of Gully No. II was greater than that of Gully No. I. This may have resulted from rapid soil water storage and drainage producing intensive runoff at the head cut of Gully No. II. The erosion of steep slopes is mainly due to gravitational mass wasting. For Gully No. II, erosion per unit area during the snowmelt season was significantly greater than that during the rainy season. During the snow-melting season, the erosion per unit area for the slope in Gully No. II was greater than that in Gully No. I. Although erosion per unit area during the rainy season for Gully No. I was higher than that of Gully No. II, the difference was negligible compared to that in the snow-melting season. The slopes of the permanent gully were steep, and the stability of the slope primarily depended on the soil suction stress as a function of the hydromechanical properties and the soil moisture.

As the channel bed erosion was closely correlated with the hydrological process and the slope erosion corresponded to the soil suction stress, further examination of the associated soil water storage and drainage and the hydromechanical properties of the soil mass in the two permanent gullies was conducted. One of the differences in the hydrological processes in the head cut indicates that soil water storage and drainage occur during the rainy season. Water drainage was absent during the snowmelt season. These results are due to the continuous melting of water from snow and ice in macropores and fissures. Once the melting process was completed, the soil water storage process ceased with the onset of the water drainage process during the transition time between the snow melting and rainy seasons.

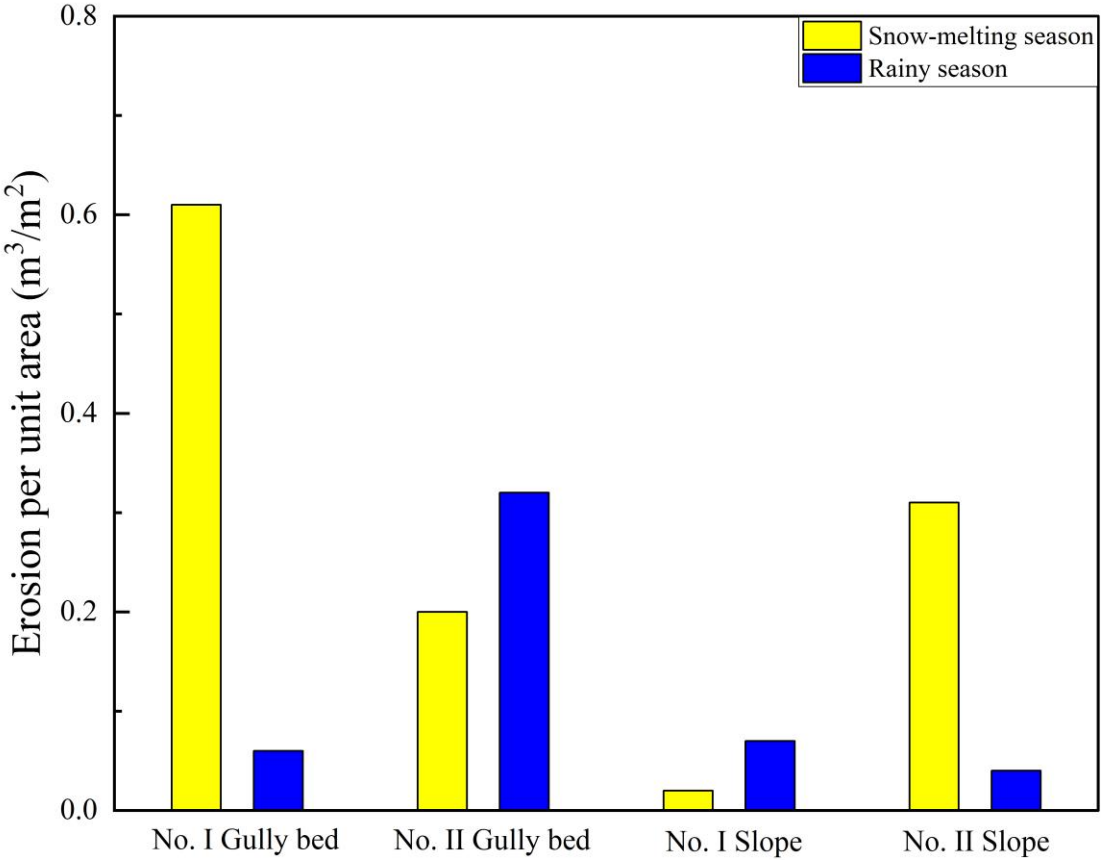

Fig. 4. Differences in the erosion per unit area for the gully bed and slope

Table 2. The physical properties and pore water pressure changes in the soil mass

Parameters	Definition	Confining pressure (kPa)	Permanent gully	
			No. I	No. II
$v_{\uparrow}$ (kPa/min)	Pore water rising ratio	100	11.83	23.04
		200	4.86	90.52
		300	5.55	10.92
$b_{\uparrow}$	Pore water rising proxy as Eq. (1)	100	0.23	0.25
		200	0.24	0.46
		300	0.30	0.41
$v_{\downarrow}$ (kPa/h)	Pore water dissipation ratio	100	3.68	22.77
		200	3.32	194.47
		300	3.66	23.94
$b_{\downarrow}$ ($\times 10^{-5}$)		100	9.97	79.70

	Pore water dissipation proxy as Eq. (2)	200	7.80	79.40
		300	6.82	18.10
c (kPa)	Effective cohesion		11.3	7.2
φ (°)	Effective friction angle		16.3	21.3
γ (kN m^{-3})	Unit weight		14.1	12.5

4.2 Physical properties of mollisols

4.2.1 Pore water pressure rising and dissipation

Under the same confining pressure, pronounced differences were observed in the rising and dissipation ratios of the pore water pressure within the mollisols of the two gullies. The pore water pressure results during the consolidation process at effective confining pressures of 100, 200, and 300 kPa were compared (Fig. 5). The physical properties and the rising and dissipation ratios and proxies are listed in Table 2. The peak value of the pore water pressure within the mollisols of Gully No. I was higher than that in Gully No. II. The peak value of the pore water pressure within the mollisols of Gully No. II increased to 57.6, 139.0, and 141.7 kPa under the confining stresses of 100, 200, and 300 kPa, respectively. In contrast, the peak value of the pore water pressure within the mollisols of Gully No. I increased to 87.9, 176.1, and 237.3 kPa, respectively.

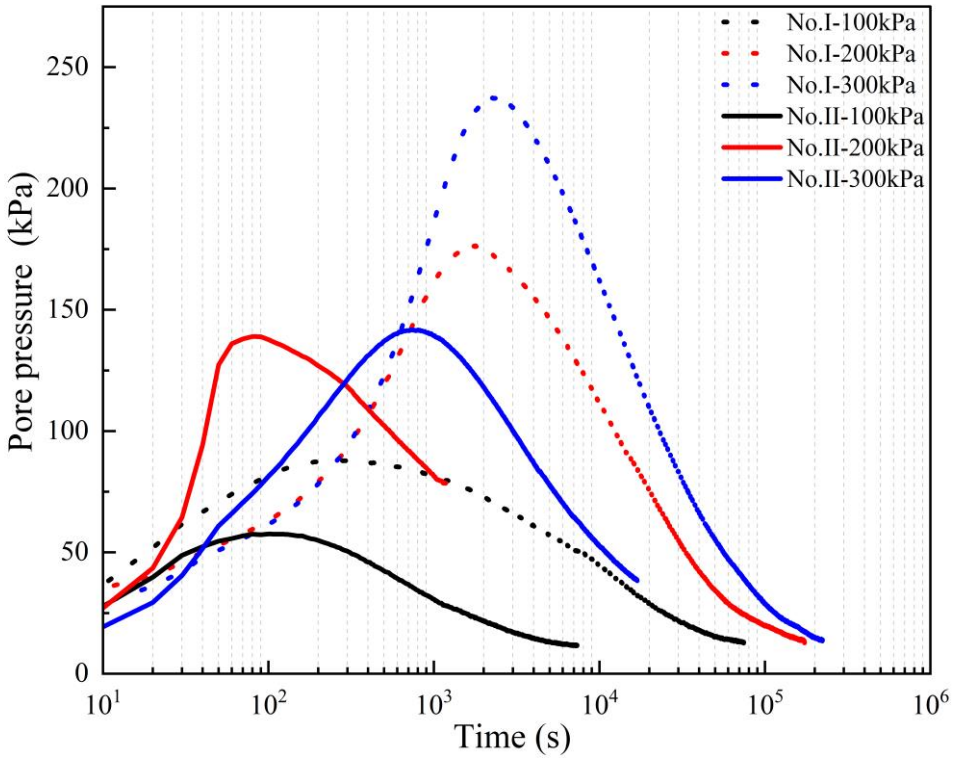

Fig. 5. Variation in pore water pressure under effective confining pressure of 100, 200, and 200 kPa by GDS triaxial shear tests (GDS Instruments, UK). The proxy for the pore water pressure rising and dissipation are calculated using Eqs. (1) and (2). The rising and dissipation ratio is calculated using the pore water pressure difference during a given time interval. The values of proxy and ratio are shown in Table 2.

The high peak pore water pressure illustrates that the mollisols of Gully No. II had strong hydraulic conductivity as the ratio increased, and the proxy and dissipation ratio and proxy represented the pore connectivity. During the rising stage, the rising ratio of the mollisols in Gully No. II was 2 to 18.6 times greater, and its rising proxy was 1.08 to 1.92 times larger than that of Gully No. I. Within the dissipation stage, the ratios were 6.20 to 58.6 greater, and

its proxies were 2.65 to 8.0 times larger than those for mollisols of Gully No. I. The largest difference between these two gullies was observed under a confining stress of 200 kPa. Therefore, the increase in the pore water pressure and dissipation properties suggests that the head cut of Gully No. II may have exhibited active hydrological processes.

4.2.2 Hydromechanical properties of mollisols

Fig. 6 shows the results of the TRIM tests, SWCC, HCF, and estimated suction stress with varying degrees of saturation. The water outflow mass was measured at 10-min intervals during the drying and wetting processes. The SWCC and HCF of the drying process and wetting process differ because water flow from the drying process relates to the applied suction level, while the water flow during the wetting process was measured at a positive pressure head (Lu and Godt, 2013). The water outflow masses measured for the mollisols in Gully No. II were generally higher than those of the mollisols in Gully No. I. For the drying tests using mollisols from Gully No. II and No. I, the water outflow masses were 0.0713 and 0.060 g per 10 min, respectively. For the wetting tests, the water outflow masses were 0.031 and 0.0208 g per 10 min, respectively (Fig. 6a). Overall, the permeability of mollisol Gully No. II was higher than that of mollisol Gully No. I. The same results were obtained for the pore water pressure increase, dissipation ratio, and proxy, as shown in Table 2.

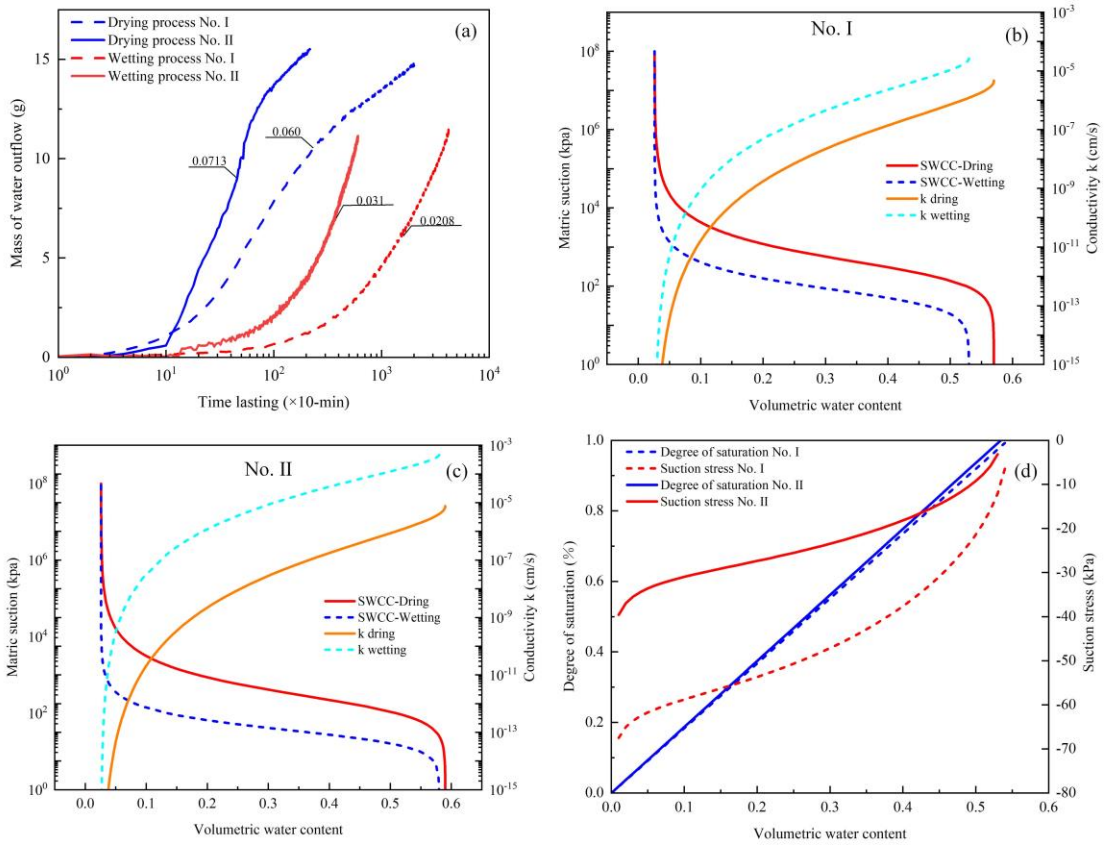

Fig. 6. Differences in the hydromechanical properties of the two soil masses. **(a)** Water flow mass in the drying and wetting process. **(b)** SWCC for soil mass of permanent Gully No. I. **(c)** SWCC for soil mass of permanent Gully No. II. **(d)** Suction stress–volumetric water content curves for the two soil masses. The mass of water outflow was recorded at 10 min for each test.

Using the parameters listed in Table 3, the SWCC and HCF curves of the mollisols were plotted (Figs. 6b and 6c). Air-entry pressure and residual water content are two important parameters that describe the hydrological and mechanical characteristics of mollisols. The air-entry pressure represents the critical value at which air enters the

saturated soil and begins to drain. In comparison, the values of α^d and α^w together prove the required air-entry pressure for mollisols in Gully No. I was greater than that in Gully No. II, the differences were 79.4 kPa and 28.0 kPa under drying and wetting conditions, respectively (Table 3). Therefore, water infiltration into Gully No. II, during either the rainy or snow-melting seasons, was more active than in Gully No. I. The residual moisture did not vary markedly due to the soil type similarity.

The saturated hydraulic conductivities of the mollisols in Gully No. I were lower than those in Gully No. II in both the drying and wetting processes. In Table 2 and Fig. 5, the pore water pressure rising ratio and proxy and the dissipation ratio and proxy further indicate the permeability of the mollisols in Gully No. II was higher than that in the mollisols of Gully No. I. Therefore, the pore water pressure changed with varying confining stress, air-entry pressure, and saturated hydraulic conductivities under drying and wetting conditions, suggesting that it is more challenging for the mollisols in Gully No. I to absorb and drain more water compared to mollisols in Gully No. II.

Figs. 6b and 6c present the matric suction and hydraulic conductivity at various soil moisture levels. However, it was impossible to compare the suction stress level with various hydrological and mechanical parameters, as listed in Table 3. Hence, the suction stress at various soil moisture levels was determined (Fig. 6d). The absolute suction stress at the specified soil moisture for mollisols in Gully No. I was higher than that of mollisols in Gully No. II, suggesting a higher possibility of gravitational mass wasting for the mollisols in Gully No. II.

Table 3. Parameters describing the SWCC and the HCF from Hydrus 1D.

Parameters	Definition	Permanent gully	
		No. I	No. II
θ_r	Residual moisture	0.0262	0.0259
θ_s^d	Saturated moisture	0.57	0.59
θ_s^w		0.53	0.58
α^d(kPa^{-1})	The inverse of the air-entry pressure head	0.0042	0.0063
α^w(kPa^{-1})		0.0183	0.0375
n^d	The pore size distribution parameter	1.69	1.68
n^w		1.95	1.91
K_s^d(cm s^{-1})	Saturated hydraulic conductivity	4.73×10^{-6}	7.82×10^{-6}
K_s^w(cm s^{-1})		2.64×10^{-5}	4.26×10^{-4}

Notes: the superscript d and w indicate drying and wetting states.

4.3 Hydrological response

4.3.1 Monitoring results

In total, 24 light rain events, two moderate rain events, five torrential rain events, and one rainstorm event were recorded (Fig. 7a). During the snow-melting season, the air temperature started to increase above 0 ℃ on March 20 with an increasing gradient of 0.15 ℃ per day, which reached 2.3 ℃ per day after April 23 (Fig. 7b). For soil moisture changes, the volumetric water content at a depth of 20 cm for Gully No. II greatly increased from April 23, whereas it only slightly increased for Gully No. I. This suggests that the head cut of the Gully No. II may have experienced higher soil moisture levels. Soil moisture throughout the rainy and snowmelt seasons had dissimilarities between sites. During the rainy season, the volumetric water content at a depth of 20 cm persistently remained at a

lower level of soil moisture than at the other three soil depths, as shown in Fig. 7c. However, during the snow-melting season, the volumetric water content of the 40 cm soil layer was the highest (Fig. 7d). Overall, the soil moisture content of Gully No. II exhibited greater fluctuations than Gully No. I in both the rainy and snowmelt seasons. Water infiltration from rain events or snowmelt into the head cut of Gully No. II was more active than that of Gully No. I. The observed difference proves that the stored and drained water from the head cut of Gully No. II was significantly greater than that in Gully No. I.

To further analyze the differences in water infiltration during the rainy and snowmelt seasons, the rate of soil moisture increase at a depth of 20 cm was compared in detail (Fig. 8). Among the four types of rain events, the mean rate of increase for Gully No. II were 0.027, 0.053, 0.102, and 0.356, respectively, which were 1.12, 1.35, 1.34, and 1.78 larger than those for Gully No. I (Figs. 8a and 9a). During the snow-melting season, soil moisture ratios increase in the initial, medium, and final stages for Gully No. II were 3.48, 1.60, and 1.66 times, respectively, than those in Gully No. I (Fig. 8b). Therefore, the water infiltration ratios for the head cut areas of Gully No. II during the rainy and snowmelt seasons.

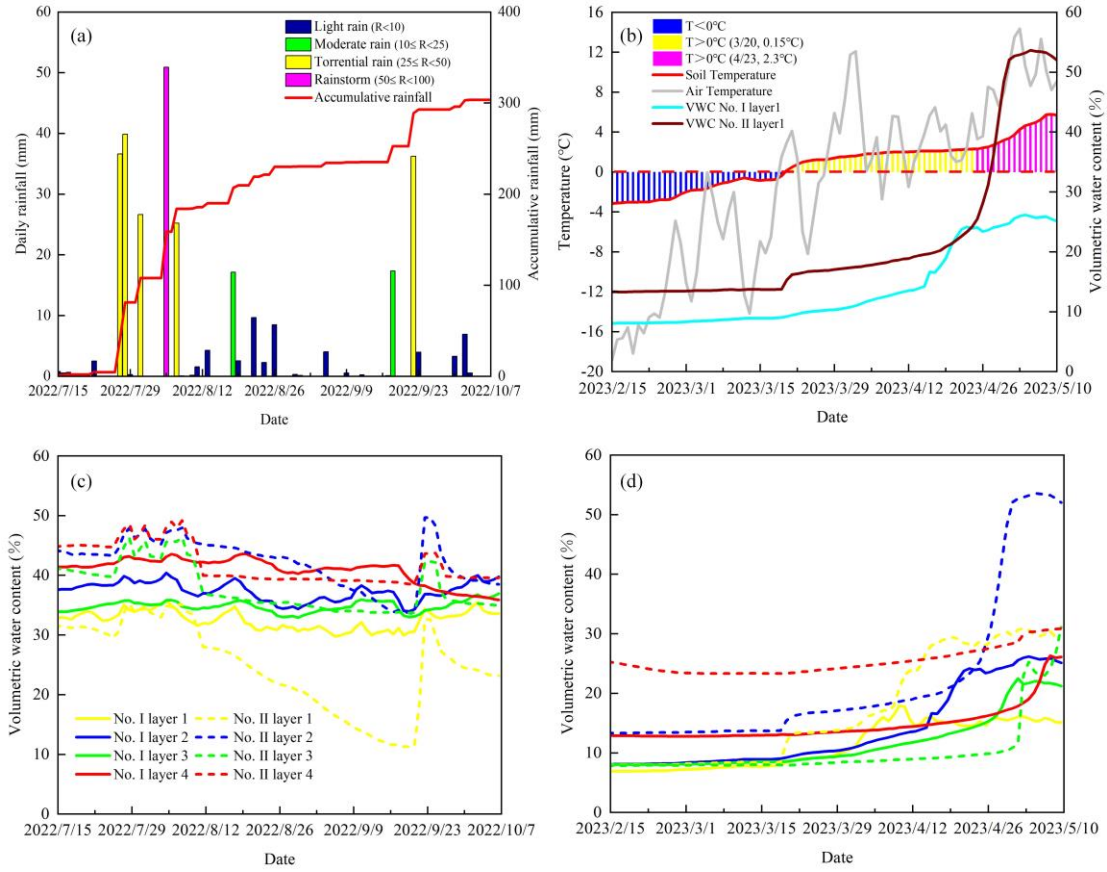

Fig. 7. Field-monitored rainfall conditions, air and ground temperature, and volumetric water content. **(a)** Rain events during the rainy season. **(b)** Soil, air temperature, and volumetric water content during the snow-melting season. **(c)** and **(d)** Monitored volumetric water content during the rainy and snow-melting seasons.

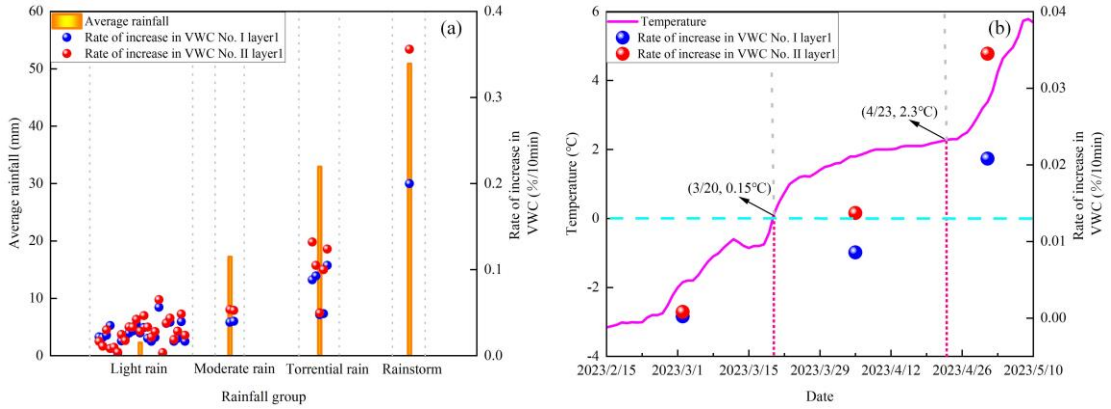

Fig. 8. Volumetric water content increasing ratio in snow-melting ratio and the rainy season. (**a**) Rate of increase in VWC at varied rain events. **(b)** Rate of increase in VWC at three stages of temperature increase.

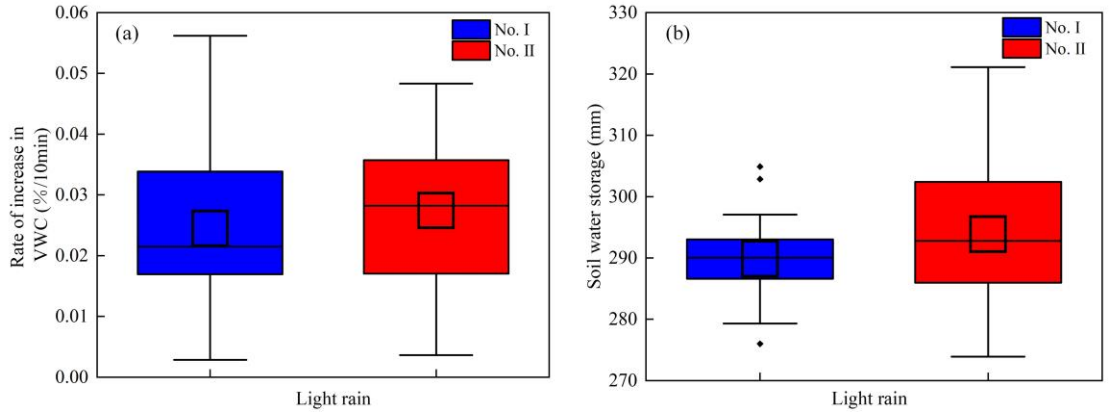

Fig. 9. Hydrologic behavior for gully head cut during light rain events. (**a**) Lower rate of increase in VWC for Gully No. I. **(b)** Higher soil water storage for Gully No. II. The three crossing lines of the boxes show the 75th quantile (Q_3), median (Q_2), and 25th quantile (Q_1) from top to bottom. The length of the box is referred to as the interquartile range (IQR = $Q_3 - Q_1$). The crossed square inside the box is the average value. The upper and lower limits of whiskers are Q_3+1.5IQR and Q_3–1.5IQR, respectively. The solid squares are the outliers.

4.3.2 Soil water storage and drainage

Fig. 10 shows the stored and drained water in the soil column at the head cuts of the two gullies. During the snowmelt season, the water stored in Gully No. II was higher than that in Gully No. I. The stored water ratio was calculated by dividing the amount of water stored in Gully No. II based on the amount stored in Gully No. I was typically larger than 1.0 throughout the snowmelt season (Fig. 10a). This ratio increased abruptly from April 26. Therefore, the amount of water stored in the head cuts of Gully No. II was higher.

Regarding the four types of rain events, the mean stored water for the head cuts of Gully No. II during the 24 light rain events was greater than that in Gully No. I (Figs. 9b and 10b). The differences in water stored in the head cuts of the two gullies were 4.0, 8.1, 15.2, and 46.3 mm, respectively. Therefore, the stored water, either in the snow-melting or rainy seasons, was higher in the head cuts of Gully No. II. However, the water stored in the head cuts of Gully No. II was not always higher than that in Gully No. I, as shown in Fig. 10c. From August 26 to September 3, 2022, the water stored at the head cut of Gully No. II was lower than that in Gully No. I. This could be attributed to high temperatures and light rain events. However, the water stored in the head cuts of Gully No. II exceeded that of Gully No. I during a torrential rainfall event on September 22. The soil water storage capacity of Gully No. II has stronger fluctuations. Rapid water infiltration generally occurs with rapid water drainage. Fig. 10d shows the water

drainage and drainage ratios of the two gullies during the rainy season. The water drained from Gully No. II was higher than that in Gully No. I. Therefore, the head cut area of the Gully No. II had better soil water storage capability in snowmelt and rainy seasons and more rapid water drainage in the rainy season than Gully No. I.

In summary, rapid soil water storage and drainage for the head cuts of Gully No. II during torrential rain or rainstorms coincided with the observed pore water pressure rise and dissipation and the hydromechanical properties of mollisols. The high permeability of mollisols at the head cut of Gully No. II was attributed to more rapid soil water storage, drainage processes, and stored water. This could considerably influence the erosion intensity of the steep slope and gully bed of the permanent gully.

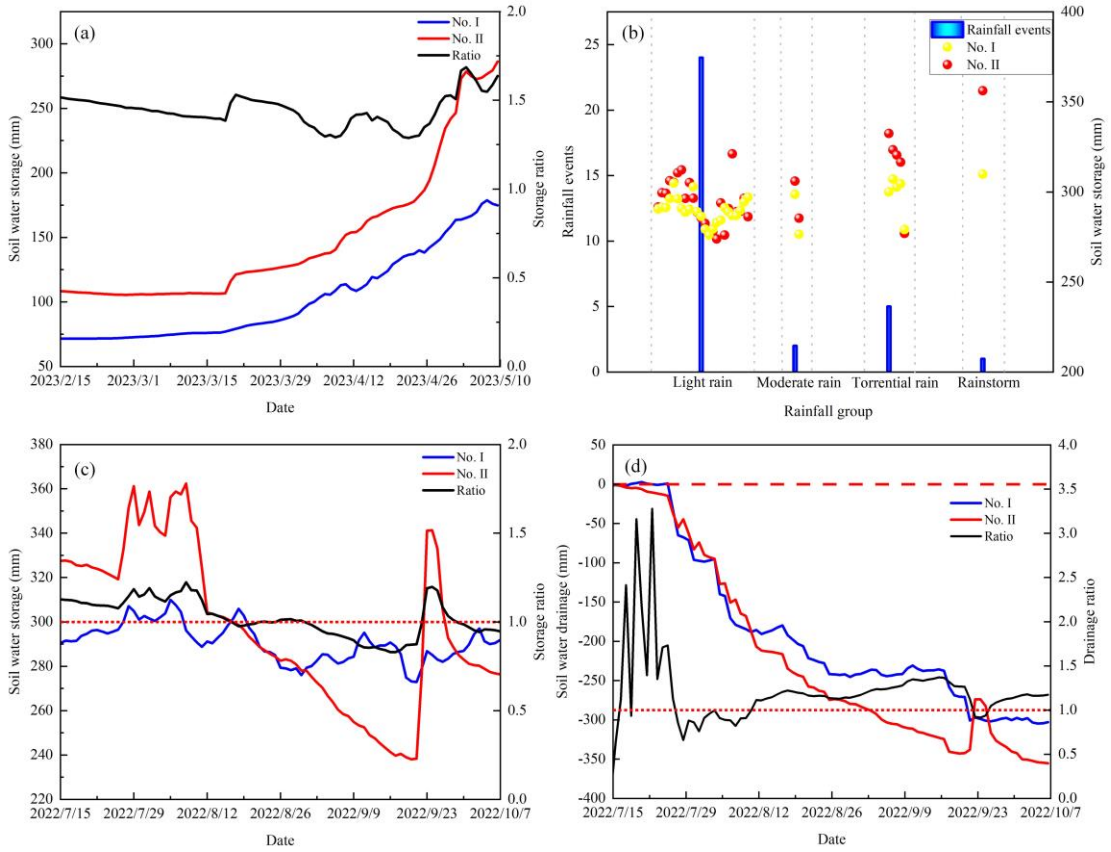

Fig. 10. Hydrological response during the rainy and snow-melting season. **(a)** Soil water storage and the storage ratio during the snow-melting season. **(b)** Soil water storage at varied rain events. **(c)** Soil water storage and the storage ratio for the two permanent gullies. **(d)** Soil water drainage and the drainage ratio during the rainy season. During the rainy season, soil water storage and drainage synchronously change with the onset and end of rainfall.

4.4 Hydromechanical response and soil loss

The mollisols in the head cut area of the two permanent gullies differed in hydromechanical properties, so the monitored soil moisture varied greatly in the field. The suction stress was estimated according to the field-monitored soil moisture at each site and the relationship between the soil moisture and matric suction (Figs. 6d, 7c, and 7d). During the rainy season, the absolute value of the suction stress of the mollisols in Gully No. II was lower than that of Gully No. I (Fig. 11a). The smaller absolute values of the suction stress for the mollisols of Gully No. II during the snowmelt season (Figure 11b). Moreover, the smaller suction stress in the snowmelt season may have resulted in strong erosion on the slope of Gully No. II, as shown in Fig. 4.

As the hydrological process of the head cut area is closely related to channel bed erosion, the hydromechanical

response influences slope stability. It is important to analyze the possible relationship between the erosion per unit area on the channel bed, soil water storage, and erosion of a steep slope with suction stress. Generally, a high absolute value of the suction stress is associated with strong, cohesive forces between the soil particles, which is a sign of stability. In contrast, a low absolute value of suction stress suggests a higher potential for slope failure. Therefore, the relationship between the absolute value of the suction stress and erosion per unit area could be negative. Fig. 11c shows the reciprocal relationship between the suction stress and erosion per unit area of the slope. The empirical relationship indicates that gravitational mass wasting occurred on the slope, and the permanent gully expanded when the suction stress remained relatively low for a prolonged period, particularly at approximately 5.6 kPa for the study area.

Erosion of the channel bed is closely related to runoff discharge during erosive rain events. During erosive rain events, the amount of stored soil water decreases runoff amount and intensity. The less rainwater stored during erosive rain events, the higher the runoff amount or the more intensive the channeled flow. Therefore, the relationship between the soil water storage and erosion per unit area of the channel bed could be negative. Fig. 11d shows the reciprocal relationship between erosion per unit area of the channel bed and soil water storage. It indicates that excessive rainwater in erosive rain events could create intensified channeled flow to erode the channel bed if the stored water in the mollisols reached a threshold, such as 139.3 mm, in this study area.

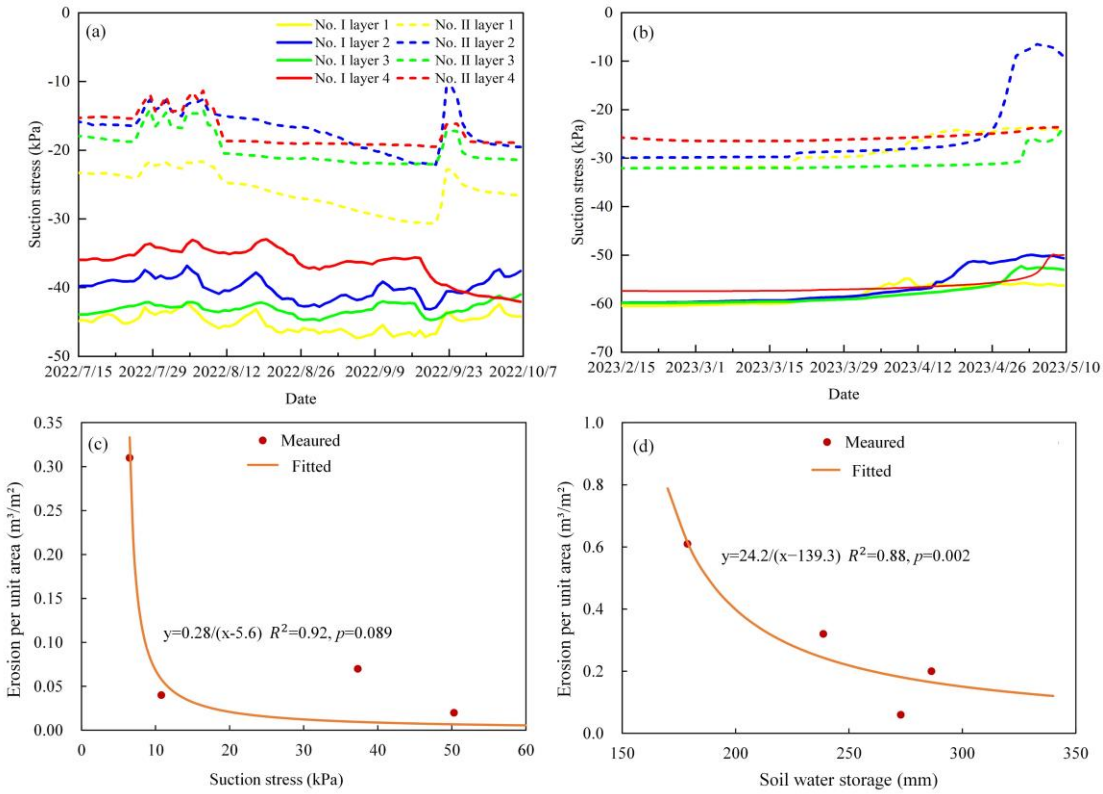

Fig. 11. Relationship between hydrology and the hydromechanical state with the erosion per unit area over approximately 3 months. **(a)** Suction stress during the rainy season. **(b)** Suction stress during the snow-melting season. **(c)** erosion per unit area on the slope decreases with suction stress. **(d)** The erosion per unit area on the channel bed decreases with the amount of soil water storage. The time for the monitored rainy and melting seasons were 111 d and 97 d.

5 Discussion

The physical processes of permanent gully development can be categorized into gravitational mass wasting on

steep slopes and sediment delivery on channel beds (Montgomery and Dietrich, 1992; van Beek et al., 2008; Luffman et al., 2015). Traditionally, most studies on gully erosion have focused on soil loss owing to water erosion and piping. Soil loss estimation is typically determined by several primary factors, such as the upslope contributing area, topographic conditions, erosive rainfall factors, and land use conditions (Li et al., 2015; Xu et al., 2017; Wang et al., 2021; Tang et al., 2022). The physical mechanics of bed erosion and slope erosion differ, making it challenging to accurately predict soil loss on steep slopes. The gravitational mass-wasting process on a slope differs from that of rainfall-induced shallow landslides, especially for those without failure planes (Poesen et al., 1998; Guo et al., 2020). However, they share similarities, such as decreased soil strength due to water infiltration (Guo et al., 2019). Thus, a thorough mechanical analysis is necessary to understand the physical processes of gravitational mass wasting on the slope and sediment delivery on the channel bed.

This study thoroughly investigated the effects of hydrological factors and hydromechanical properties on soil loss on both slopes and channel beds. Mass failure on the hillslopes was governed by suction stress. Meanwhile, erosion on the channel beds was influenced by the soil water storage or runoff amount. Therefore, hydrological factors related to soil water storage and drainage were analyzed (Fig. 10), along with volumetric changes at various rain events and snow-melting stages (Fig. 8). In this study, we also investigated the hydromechanical properties and pore water pressure at a given confining stress (Table 2 and Fig. 5), the relationship between the saturation degree and suction stress (Fig. 6), and estimated the suction stress variation during the rainy and snow-melting seasons (Figs. 11a and 11b). Field observations revealed two permanent gullies with distinct erosion on the slope and gully beds. Gully No. II shows signs of head cut disruption, in contrast to Gully No. I, resulting in disparities in erosion per unit area for both seasons and sites. The hydromechanical properties of the mollisols are distinct between the two gullies, directly affecting water movement. This is evident from the increase in pore water pressure, dissipation ratio, and proxy. In the head cut of Gully No. II, the mollisols were significantly disturbed, and the soil mass had higher permeability and lower suction stress at a given saturation degree. This finding indicates more active water infiltration compared to Gully No. I was triggered by changes in the soil's capacity to store and release water and the higher volumetric water content increasing ratio. Therefore, the head cut area of Gully No. II underwent more aggressive hydrological processes. Additionally, the observed rainfall amount of 139.3 mm in this study was smaller than the 177 mm proposed by Tang et al. (2023). This could be explained by the different capacities for plant interception and depression detention during the rainy season.

The soil water storage and drainage capacity at the head cut considerably influenced soil loss. Although this study focused primarily on soil water storage and its impact, runoff was not addressed. The soil water storage and runoff depth were approximately equal to the rainfall depth from the water balance perspective. Consequently, the erosion per unit area of the channel bed was inversely proportional to the soil water storage, as shown in Fig. 11d. Some researchers have identified factors leading to the erosion of mass failures on steep slopes, such as long-duration storms (Xu et al., 2020), initial soil moisture in the pre-winter season (Wen et al., 2024), presence of tensile crack morphology (Zhou et al., 2023) and heaving and thawing (Thomas et al., 2009). The head cut of Gully No. II has a high level of disturbance, which may result in higher permeability, quicker water pressure response, and higher soil moisture during the rainy or snowmelt seasons. Meanwhile, the soil suction stress was lower, and slope erosion was more intense than that of Gully No. I. The distance between the two gullies was only 1.4 km, and the climatic conditions were similar. Therefore, soil properties may be the dominant intrinsic factors governing soil loss on gully slopes.

Commonly, the gully bed erosion rates mainly depend on runoff intensity, and some studies reported that the runoff hydraulics in the rainy season were significantly higher than the snow-melting runoff. However, additional studies proved that gully heads may retreat faster in the snow-melting season than in the summer (Wu et al., 2008; Hu et al., 2009). The accumulated snowfall depth during the monitoring duration in this study was high, up to 49.6

mm, which was far more than the average snow depth of 30 mm. Besides, the snowfall melted from 3 to 10 May 2023 (Figs. 7a and 7b). Therefore, heavy snowfall during the winter of 2022 and early spring of 2023 and the intensive melting may result in high soil moisture and intensive runoff, ultimately causing substantial bed erosion. Long-term saturation during the snowmelt season provides sufficient water infiltration and low suction stress. Therefore, the highest erosion per unit area occurred in the snowmelt season but not in the rainy season.

Dong et al. (2011) revealed that a critical mass water content for gravitational mass wasting ranged from 31.0% to 33.8%, corresponding to a volumetric water content of 39.0% to 48.0% for the soil mass and a suction stress of 11.0 kPa. This showed that the direct-shear apparatus limited the ability to differentiate between the effective cohesion and suction stress contributions to total cohesion. As shown in Fig. 10b and supported by Xu et al. (2020), the high soil water storage during the snow-melting season in Gully No. II (Fig. 9a) and long-term water infiltration can lower suction stress and higher erosion per unit area. This suggests a potentially reciprocal relationship between the absolute suction stress and erosion per unit area. The result shown in Figs. 11c and 11d are key findings and main contributions in the study domain of gully erosion, as they clarify the role of suction stress of storied water on soil loss from steep slopes and gully beds, respectively. Our results also imply that the soil water storage may not equal the amount of rainfall from the event, but instead partially derives from the initial soil water. Figure 11 illustrates that antecedent soil moisture or precipitation substantially influences surface runoff depth and soil loss during the permanent gully expansion in MEC, while this critical aspect has been neglected in previous study. In other words, the effect of antecedent precipitation should be assessed in predicting soil loss as it closely relates to the soil water and indirectly influences the runoff generation and intensity (Sachs and Sarah, 2017; Wei et al., 2017; Schoener and Stone, 2019; Wang et al., 2019). Notably, the theoretical framework underlying this work is that the soil loss at steep slopes occurs through the mechanism of bank slope stability, and the loss in gully beds occurs due to the balance between the shear force from runoff water and soil erodibility. Therefore, it is preferrable to predict soil loss in the permanent gullies from soil water storage and the hydromechanical response of soil mass, rather than solely from rainfall amount.

6 Conclusions

Permanent gully development is a hydrogeomorphic phenomenon, and its physical mechanics can be attributed to the hydrological and hydromechanical responses of the head cut. In the mollisol region of Northeast China, numerous studies on gully development have focused on soil loss in response to rainfall or snow depth. However, relatively few studies have addressed the physical mechanics of gravitational mass wasting. This study has provided a complete analysis of soil loss on steep slopes and channel beds in two permanent gullies according to hydrological processes, such as infiltration, soil water storage, drainage, and hydromechanical responses, such as changes in suction stress levels. The following conclusions were drawn:

(1) Mollisols in the head-cut areas of Gully No. II exhibited a higher permeability than Gully No. I. This can be attributed to the elevated ratio and proxy for pore water pressure rise and dissipation. The TRIM test results confirmed that the saturated mollisols in the Gully No. II drain faster than Gully No. I, owing to their higher air-entry pressure and saturated hydraulic conductivity during the wetting and drying cycles.

(2) The head cut area of Gully No. II exhibited more intense hydrological processes than Gully No. I. This could be explained by the higher ratio of soil moisture increase observed during the four rain event types and three snow-melting stages. Soil water storage in Gully No. II experienced greater fluctuations during torrential rains and rainstorms. Overall, the absolute suction in Gully No. II remained lower than that in Gully No. I, potentially triggering greater erosion on the steep slopes.

(3) The relationships between erosion per unit area on the steep slope and channel bed were analyzed for the suction stress and soil water storage. Our findings indicate that low suction stress and high soil water storage can

increase gravitational mass wasting while reducing erosion on the channel bed. The two empirical relationships and their efficiency can be enhanced by incorporating data from ongoing monitoring efforts to enhance the prediction of future soil loss.

Acknowledgments

This work was supported by the National Key Research and Development Program (Grant No. 2021YFD1500700). The authors extend their gratitude to the colleges at the Jiusan Soil and Water Conservation Experimental Station, Beijing Normal University, for their help during field investigations.

Code and data availability

The corresponding author, Prof. Chao Ma, is willing to share the raw/processed data upon reasonable request.

Author contributions

Prof. Ma conceived the study based on his skills in gravitational mass-wasting and unsaturated soil mechanics and proposed the concept of hydrology and hydromechanical conditions in analyzing gravitational mass-wasting. Under the guidance of Prof. Ma, Mr. Dongshuo Zheng and Shoupeng Wang conducted indoor tests of soil strength and hydraulic-mechanical properties. Prof. Zhang helped determine the field observation sites. Dr. Dong gave insightful comments. Dr. Jie Tang and Yanru Wen provided the research progress about the gravitational mass wasting on gully expansion in the study area.

Competing interests

The authors declare no conflicts of interest.

References

[1] Allen, P. M., Arnold, J. G., Auguste, L., White, J., and Dunbar, J.: Application of a simple headcut advance model for gullies, Hydrol. Earth Syst. Sci., 43, 202-217, https://doi.org/10.1002/esp.4233, 2018.

[2] Bierman, P. R. and Montgomery, D. R.: Key Concepts in Geomorphology, W. H. Freeman and Company Publishers, ISBN 13:9781429238601, 2014.

[3] Dong, Y., Wu, Y., Yin, J., Wang, Y., and Gou, S.: Investigation of Soil Shear-Strength Parameters and Prediction of the Collapse of Gully Walls in the Black Soil Region of Northeastern China, Phys. Geogr, 32, 161-178, https://doi.org/10.2747/0272-3646.32.2.161, 2011.

[4] Dong, Y., Wu, Y., Qin, W., Guo, Q., Yin, Z., and Duan, X.: The gully erosion rates in the black soil region of northeastern China: Induced by different processes and indicated by different indexes, Catena, 182, https://doi.org/10.1016/j.catena.2019.104146, 2019.

[5] Evans, D.: Geomorphology: Critical Concepts in Geography - Volume IV, Glacial Geomorphology, Routledge., ISBN 9780415641708, 2004.

[6] Fan, H., Hou, Y., Xu, X., Mi, C., and Shi, H.: Composite Factors during Snowmelt Erosion of Farmland in Black Soil Region of Northeast China: Temperature, Snowmelt Runoff, Thaw Depths and Contour Ridge Culture, Water, 15, https://doi.org/10.3390/w15162918, 2023.

[7] Farkas, C., Randriamampianina, R., and Majercak, J.: Modelling impacts of different climate change scenarios on soil water regime of a Mollisol, Cereal Res. Commun., 33, 185-188, https://doi.org/10.1556/crc.33.2005.1.45, 2005.

[8] Gómez-Gutiérrez, A., Schnabel, S., De Sanjosé, J. J., and Contador, F. L.: Exploring the relationships between gully erosion and hydrology in rangelands of SW Spain, Z. Geomorphol, 56, 27-44,

https://doi.org/10.1127/0372-8854/2012/s-00071, 2012.

[9] Guan, Y., Yang, S., Zhao, C., Lou, H., Chen, K., Zhang, C., and Wu, B.: Monitoring long-term gully erosion and topographic thresholds in the marginal zone of the Chinese Loess Plateau, Soil Tillage Res., 205, https://doi.org/10.1016/j.still.2020.104800, 2021.

[10] Guo, W., Xu, X., Wang, W., Zhu, T., and Liu, Y.: Experimental study of shallow mass movements on gully slopes and associated sediment under rainfall on the Chinese loess plateau, Geomorphology, 350, https://doi.org/10.1016/j.geomorph.2019.106919, 2020.

[11] Guo, W., Luo, L., Wang, W., Liu, Z., Chen, Z., Kang, H., and Yang, B.: Sensitivity of rainstorm-triggered shallow mass movements on gully slopes to topographical factors on the Chinese Loess Plateau, Geomorphology, 337, 69-78, https://doi.org/10.1016/j.geomorph.2019.04.006, 2019.

[12] Harmon, R. S.and Doe, W. W.: Landscape erosion and evolution modeling, Springer Science + Business Media, New York., ISBN 978-1-4613-5139-9, 2001.

[13] Hu, G., Wu, Y., Liu, B., Yu, Z., You, Z., and Zhang, Y.: Short-term gully retreat rates over rolling hill areas in black soil of Northeast China, Catena, 71, 321-329, https://doi.org/10.1016/j.catena.2007.02.004, 2007.

[14] Hu, G., Wu, Y., Liu, B., Zhang, Y., You, Z., and Yu, Z.: The characteristics of gully erosion over rolling hilly black soil areas of Northeast China, J Geogr Sci., 19, 309-320, https:// 10.1007/s11442-009-0309-4, 2009.

[15] Hayas, A., Peña, A., and Vanwalleghem, T.: Predicting gully width and widening rates from upstream contribution area and rainfall: A case study in SW Spain, Geomorphology, 341, 130-139, https://doi.org/10.1016/j.geomorph.2019.05.017, 2019.

[16] Jiao, J., Qin, W., Li, K., Xu, H., Yin, Z., and Hou, S.: Critical thresholds for stage division of water erosion process in different ridge systems in mollisol region of Northeast China, J Mt. Sci., 20, 1540-1560, https://doi.org/10.1007/s11629-022-7476-5, 2023.

[17] Kirkby, M. J. and Bracken, L. J.: Gully processes and gully dynamics, Earth Surf. Process. Landf., 34, 1841-1851, https://doi.org/10.1002/esp.1866, 2009.

[18] Li, H., Cruse, R. M., Liu, X., and Zhang, X.: Effects of Topography and Land Use Change on Gully Development in Typical Mollisol Region of Northeast China, Chin. Geogr. Sci., 26, 779-788, https://doi.org/10.1007/s11769-016-0837-7, 2016.

[19] Li, H., Shen, H., Wang, Y., Wang, Y., and Gao, Q.: Effects of Ridge Tillage and Straw Returning on Runoff and Soil Loss under Simulated Rainfall in the Mollisol Region of Northeast China, Sustainability, 13, https://doi.org/10.3390/su131910614, 2021.

[20] Li, Z., Zhang, Y., Zhu, Q., He, Y., and Yao, W.: Assessment of bank gully development and vegetation coverage on the Chinese Loess Plateau, Geomorphology, 228, 462-469, https://doi.org/10.1016/j.geomorph.2014.10.005, 2015.

[21] Li, Z., Zhang, Y., Zhu, Q., Yang, S., Li, H., and Ma, H.: A gully erosion assessment model for the Chinese Loess Plateau based on changes in gully length and area, Catena, 148, 195-203, https://doi.org/10.1016/j.catena.2016.04.018, 2017.

[22] Liu, X., Guo, M., Zhang, X., Zhang, S., Zhou, P., Chen, Z., Qi, J., and Shen, Q.: Morphological characteristics and volume estimation model of permanent gullies and topographic threshold of gullying in the rolling hilly Mollisols region of northeast China, Catena, 231, https://doi.org/10.1016/j.catena.2023.107323, 2023.

[23] Lu, N. and Godt, J. W.: Hillslope Hydrology and Stability, Cambridge University Press, Cambridge, https://doi.org/DOI:10.1017/CBO9781139108164, 2013.

[24] Luffman, I. E., Nandi, A., and Spiegel, T.: Gully morphology, hillslope erosion, and precipitation characteristics in the Appalachian Valley and Ridge province, southeastern USA, Catena, 133, 221-232, https://doi.org/10.1016/j.catena.2015.05.015, 2015.

[25] Montgomery, D. R. and Dietrich, W. E.: Channel initiation and the problem of landscape scale, Science, 255, 826-830, https://doi.org/10.1126/science.255.5046.826, 1992.

[26] Mualem, Y.: Hysteretical models for prediction of the hydraulic conductivity of unsaturated porous media, Water Resour. Res., 12, 1248-1254, https://doi.org/10.1029/WR012i006p01248, 1976.

[27] Poesen, J., Vandaele, K., and van Wesemael, B.: Gully Erosion: Importance and Model Implications. In: Boardman, J., Favis-Mortlock, D. (eds) Modelling Soil Erosion by Water. NATO ASI Series, vol 55. Springer, Berlin, Heidelberg., https://doi.org/10.1007/978-3-642-58913-3_22, 1998.

[28] Poesen, J. W. A., Torri, D. B., and Vanwalleghem, T.: Gully Erosion: Procedures to Adopt When Modelling Soil Erosion in Landscapes Affected by Gullying, in: Handbook of Erosion Modelling, 360-386, https://doi.org/10.1002/9781444328455.ch19, 2010.

[29] Rengers, F. K. and Tucker, G. E.: Analysis and modeling of gully headcut dynamics, North American high plains, J. Geophys. Res.-Earth Surf., 119, 983-1003, https://doi.org/10.1002/2013jf002962, 2014.

[30] Stein, O. R. and Latray, D. A.: Experiments and modeling of head cut migration in stratified soils, Water Resour. Res., 38, 1284, https://doi.org/10.1029/2001WR001166, 2002.

[31] Sidle, R. C., Gomi, T., Usuga, J. C. L., and Jarihani, B.: Hydrogeomorphic processes and scaling issues in the continuum from soil pedons to catchments, Earth Sci. Rev, 175, 75-96, https://doi.org/10.1016/j.earscirev.2017.10.010, 2017.

[32] Svoray, T., Michailov, E., Cohen, A., Rokach, L., and Sturm, A.: Predicting gully initiation: comparing data mining techniques, analytical hierarchy processes and the topographic threshold, Earth Surf. Process. Landf., 37, 607-619, https://doi.org/10.1002/esp.2273, 2012.

[33] Sachs, E. and Sarah, P.: Combined effect of rain temperature and antecedent soil moisture on runoff and erosion on Loess, Catena, 158, 213-218, https://doi.org/10.1016/j.catena.2017.07.007, 2017.

[34] Schoener, G. and Stone, M. C.: Impact of antecedent soil moisture on runoff from a semiarid catchment, J Hydrol., 569, 627-636, https://doi.org/10.1016/j.jhydrol.2018.12.025, 2019.

[35] Tang, J., Xie, Y., Wu, Y., and Liu, G.: Influence of precipitation change and topography characteristics on the development of farmland gully in the black soil region of northeast China, Catena, 224, https://doi.org/10.1016/j.catena.2023.106999, 2023.

[36] Tang, J., Xie, Y., Liu, C., Dong, H., and Liu, G.: Effects of rainfall characteristics and contour tillage on ephemeral gully development in a field in Northeastern China, Soil Tillage Res., 218, https://doi.org/10.1016/j.still.2021.105312, 2022.

[37] Tang, J., Liu, G., Xie, Y., Duan, X., Wang, D., and Zhang, S.: Ephemeral gullies caused by snowmelt: A ten-year study in northeastern China, Soil Tillage Res., 212, 105048, https://doi.org/10.1016/j.still.2021.105048, 2021.

[38] Tebebu, T. Y., Abiy, A. Z., Zegeye, A. D., Dahlke, H. E., Easton, Z. M., Tilahun, S. A., Collick, A. S., Kidnau, S., Moges, S., Dadgari, F., and Steenhuis, T. S.: Surface and subsurface flow effect on permanent gully formation and upland erosion near Lake Tana in the northern highlands of Ethiopia, Hydrol. Earth Syst. Sci., 14, 2207-2217, https://doi.org/10.5194/hess-14-2207-2010, 2010.

[39] Thomas, J. T., Iverson, N. R., and Burkart, M. R.: Rank-collapse processes in a valley-bottom gully, western Iowa, Earth Surf. Process. Landf., 34, 109-122, https://doi.org/10.1002/esp.1699, 2009.

[40] Torri, D. and Poesen, J.: A review of topographic threshold conditions for gully head development in different environments, Earth Sci. Rev, 130, 73-85, https://doi.org/10.1016/j.earscirev.2013.12.006, 2014.

[41] van Beek, R., Cammeraat, E., Andreu, V., Mickovski, S. B., and Dorren, L.: Hillslope Processes: Mass Wasting, Slope Stability and Erosion, in: Slope Stability and Erosion Control: Ecotechnological Solutions, edited by: Norris, J. E., Stokes, A., Mickovski, S. B., Cammeraat, E., van Beek, R., Nicoll, B. C., and Achim, A., Springer

Netherlands, Dordrecht, 17-64, https://doi.org/10.1007/978-1-4020-6676-4_3, 2008.
[42] van Genuchten, M. T.: A Closed-form Equation for Predicting the Hydraulic Conductivity of Unsaturated Soils, Soil Sci. Soc. Am. J., 44, 892-898, https://doi.org/10.2136/sssaj1980.03615995004400050002x, 1980.
[43] Vanmaercke, M., Poesen, J., Van Mele, B., Demuzere, M., Bruynseels, A., Golosov, V., Bezerra, J. F. R., Bolysov, S., Dvinskih, A., Frankl, A., Fuseina, Y., Guerra, A. J. T., Haregeweyn, N., Ionita, I., Imwangana, F. M., Moeyersons, J., Moshe, I., Samani, A. N., Niacsu, L., Nyssen, J., Otsuki, Y., Radoane, M., Rysin, I., Ryzhov, Y. V., and Yermolaev, O.: How fast do gully headcuts retreat?, Earth Sci. Rev, 154, 336-355, https://doi.org/10.1016/j.earscirev.2016.01.009, 2016.
[44] Wei, L., Zhang, B., and Wang, M.: Effects of antecedent soil moisture on runoff and soil erosion in alley cropping systems, Agr Water Manage., 94, 54-62, https:// doi.org/10.1016/j.agwat.2007.08.007, 2007.
[45] Wu, Y., Zheng, Q., Zhang, Y., Liu, B., Cheng, H., and Wang, Y.: Development of gullies and sediment production in the black soil region of northeastern China, Geomorphology, 101, 683-691, https://doi.org/10.1016/j.geomorph.2008.03.008, 2008.
[46] Wang, J., Zhang, Y., Deng, J., Yu, S., and Zhao, Y.: Long-Term Gully Erosion and Its Response to Human Intervention in the Tableland Region of the Chinese Loess Plateau, Remote Sens., 13, https://doi.org/10.3390/rs13245053, 2021a.
[47] Wang, L., Zheng, F., Liu, G., Zhang, X., Wilson, G. V., Shi, H., and Liu, X.: Seasonal changes of soil erosion and its spatial distribution on a long gentle hillslope in the Chinese Mollisol region, Int. Soil Water Conserv. Res., 9, 394-404, https://doi.org/10.1016/j.iswcr.2021.02.001, 2021b.
[48] Wang, Z., Liu, B., Wang, X., Gao, X., and Liu, G.: Erosion effect on the productivity of black soil in Northeast China, Sci. China Ser. D-Earth Sci., 52, 1005-1021, https://doi.org/10.1007/s11430-009-0093-0, 2009.
[49] Wayllace, A. and Lu, N.: A Transient Water Release and Imbibitions Method for Rapidly Measuring Wetting and Drying Soil Water Retention and Hydraulic Conductivity Functions, Geotech. Test. J., 35, 103-117, https://doi.org/10.1520/GTJ103596, 2012.
[50] Wen, Y., Kasielke, T., Li, H., Zepp, H., and Zhang, B.: A case-study on history and rates of gully erosion in Northeast China, Land Degrad. Dev., 32, 4254-4266, https://doi.org/10.1002/ldr.4031, 2021.
[51] Wen, Y., Liu, B., Jiang, H., Li, T., Zhang, B., and Wu, W.: Initial soil moisture prewinter affects the freeze-thaw profile dynamics of a Mollisol in Northeast China, Catena, 234, https://doi.org/10.1016/j.catena.2023.107648, 2024.
[52] Wang, F., Tian, P., Guo, W., Chen, L., Gong, Y., and Ping, Y.: Effects of rainfall patterns, vegetation cover types and antecedent soil moisture on run-off and soil loss of typical Luvisol in southern China, Earth Surf Process Landf., 49, 2998-3012, https://doi.org/10.1002/esp.5871, 2024.
[53] Xu, X., Zheng, F., Wilson, G. V., and Wu, M.: Upslope inflow, hillslope gradient and rainfall intensity impacts on ephemeral gully erosion, Land Degrad. Dev., 28, 2623-2635, https://doi.org/10.1002/ldr.2825, 2017.
[54] Xu, X., Zheng, F., Wilson, G. V., He, C., Lu, J., and Bian, F.: Comparison of runoff and soil loss in different tillage systems in the Mollisol region of Northeast China, Soil Tillage Res., 177, 1-11, https://doi.org/10.1016/j.still.2017.10.005, 2018.
[55] Xu, X., Ma, Y., Yang, W., Zhang, H., Tarolli, P., Jiang, Y., and Yan, Q.: Qualifying mass failures on loess gully sidewalls using laboratory experimentation, Catena, 187, https://doi.org/10.1016/j.catena.2019.104252, 2020.
[56] Yang, J., Zhang, S., Chang, L., Li, F., Li, T. Q., and Gao, Y.: Gully erosion regionalization of black soil area in northeastern China, Chin. Geogr. Sci., 27, 78-87, https://doi.org/10.1007/s11769-017-0848-z, 2017.
[57] Zare, M., Soufi, M., Nejabat, M., and Pourghasemi, H. R.: The topographic threshold of gully erosion and contributing factors, Nat. Hazard, 112, 2013-2035, https://doi.org/10.1007/s11069-022-05254-6, 2022.
[58] Zhang, S., Jiang, L., Liu, X., Zhang, X., Fu, S., and Dai, L.: Soil nutrient variance by slope position in a

Mollisol farmland area of Northeast China, Chin. Geogr. Sci., 26, 508-517, https://doi.org/10.1007/s11769-015-0737-2, 2016.

[59] Zhang, S., Wang, X., Xiao, Z., Qu, F., Wang, X., Li, Y., Aurangzeib, M., Zhang, X., and Liu, X.: Quantitative studies of gully slope erosion and soil physiochemical properties during freeze-thaw cycling in a Mollisol region, Sci. Total Environ., 707, https://doi.org/10.1016/j.scitotenv.2019.136191, 2020.

[60] Zhang, S., Han, X., Cruse, R., Zhang, X., Hu, W., Yan, Y., and Guo, M.: Morphological characteristics and influencing factors of permanent gully and its contribution to regional soil loss based on a field investigation of 393 km^2 in Mollisols region of northeast China, Catena, 217, https://doi.org/10.1016/j.catena.2022.106467, 2022.

[61] Zhou, P., Guo, M., Zhang, X., Zhang, S., Qi, J., Chen, Z., Wang, L., and Xu, J.: Quantifying the effect of freeze-thaw on the soil erodibility of gully heads of typical gullies in the Mollisols region of Northeast China, Catena, 228, https://doi.org/10.1016/j.catena.2023.107180, 2023.